

## Low offset frequency $1/f$ flicker noise in spin-torque vortex oscillators

Steffen Wittrock,<sup>1,\*</sup> Sumito Tsunegi,<sup>2</sup> Kay Yakushiji,<sup>2</sup> Akio Fukushima,<sup>2</sup> Hitoshi Kubota,<sup>2</sup> Paolo Bortolotti,<sup>1</sup> Ursula Ebels,<sup>3</sup> Shinji Yuasa,<sup>2</sup> Gilles Cibiel,<sup>4</sup> Serge Galliou,<sup>5</sup> Enrico Rubiola,<sup>5</sup> and Vincent Cros<sup>1,†</sup>

<sup>1</sup>*Unité Mixte de Physique CNRS/Thales, Université Paris-Sud, Université Paris-Saclay, 1 Avenue Augustin Fresnel, 91767 Palaiseau, France*

<sup>2</sup>*National Institute of Advanced Industrial Science and Technology, Spintronics Research Center, Tsukuba, Ibaraki 305-8568, Japan*

<sup>3</sup>*Université Grenoble Alpes, CEA, INAC-SPINTEC, CNRS, SPINTEC, 38000 Grenoble, France*

<sup>4</sup>*Centre National d'Études Spatiales, 18 avenue Edouard Belin, 31401 Toulouse, France*

<sup>5</sup>*FEMTO-ST Institute, CNRS, Université Bourgogne Franche Comté, 25030 Besançon, France*



(Received 16 November 2018; revised manuscript received 30 March 2019; published 17 June 2019)

Low-frequency noise close to the carrier remains little explored in spin-torque nano-oscillators. However, it is crucial to investigate as it limits the oscillator's frequency stability. This work addresses the low offset frequency flicker noise of a spin-torque vortex oscillator in the regime of large-amplitude steady oscillations. We first phenomenologically expand the nonlinear auto-oscillator theory, aiming to reveal the properties of this noise. We then present a thorough experimental study of the oscillator's  $1/f$  flicker noise and discuss the results based on the theoretical predictions. Thereby, we connect the oscillator's nonlinear dynamics with the concept of flicker noise and furthermore refer to the influence of a standard  $1/f$  noise description based on the Hooge formula, taking into account the nonconstant magnetic oscillation volume, which contributes to the magnetoresistance.

DOI: [10.1103/PhysRevB.99.235135](https://doi.org/10.1103/PhysRevB.99.235135)

### I. INTRODUCTION

Spin-torque nano-oscillators (STNOs) convert magnetization dynamics into electrical rf signals by exploiting fundamental phenomena of spintronics, such as the magnetoresistive effect [1,2] and the concept of spin transfer torque [3,4], which allows sustaining their dynamics. Since 2003, the investigation of STNO properties [5] has attracted huge interest as they have been considered not only as a unique opportunity for studying nonlinear dynamics at the nanoscale but also as promising candidates for next-generation multifunctional spintronic devices [6]. More recently, STNOs have also been demonstrated to be capable of being key elements in the realization of broadband microwave energy harvesting [7] and frequency detection [8,9] and of reconstructing bioinspired networks for neuromorphic computing [10,11].

These possible applications are all strongly linked to the STNO's fundamental property, i.e., its nonlinearity, which describes a coupling between the oscillator's amplitude and phase [12,13]. It provides the basis for manifold phenomena such as injection locking to an external rf signal [14,15], synchronization of multiple STNOs [16–18], and the spin-torque diode effect [8,19–21]. However, nonlinear behavior also causes the oscillator's poor spectral coherence and leads to a conversion from amplitude to phase noise [12,13,22], which limits its amplitude and frequency stability and therefore its applicability in real practical devices.

Noise mechanisms in tunnel- (TMR) or giant- (GMR) magnetoresistive-effect-based magnetic sensors, which represent the building block of a STNO, are usually the frequency-independent shot (only for TMR) and thermal noise and

low-frequency  $1/f$  noise, also called flicker noise. In certain cases, random telegraph noise (RTN), arising from the fluctuations between two different energy levels, can also exist. Its sources are mainly of electronic and/or magnetic origins and equally present in STNOs as well, where it is anticipated that the existence of self-sustained nonlinear magnetization dynamics drastically influences the noise characteristics compared to classical magnetic sensors.

The STNO's noise distribution for offset frequencies far from the carrier frequency is now reasonably well understood. At room temperature, it has been found that it is mainly attributed to dominant thermal noise in the framework of nonlinearity [13,22–24]. However, the noise at low offset frequencies, which is crucial for most of the targeted applications, remains largely under investigation. The existence of flicker noise at these low-frequency offsets is of a general nature, as noise of spectral  $1/f^\beta$  scaling is present in a wide variety of physical systems, such as stellar emissions, lake turbulence, Nile flooding, and virtually all electronic devices [25]. Initially recognized by Johnson [26] and later investigated in thin films [27], it has recently attracted attention as the dominant noise source in GMR and TMR sensors [28–31] and their major drawback in terms of performance.

In STNOs, the  $1/f$  flicker noise at low offset frequencies has so far been only experimentally recognized [22,23,32,33]. In Refs. [22,23], the focus was on thermal noise at high offset frequencies, and an indication of colored  $1/f$  noise at lower offsets was found. Reference [32] presented a measurement method to access the  $1/f$  regime and showed its influence on the frequency spectra. In Ref. [33], the study concerned  $1/f$  noise in the very specific geometry of nanocontact STNOs. A large influence on multiple present modes, which are particularly avoided within the work presented here, was found. In the present work, we systematically investigate the  $1/f$  flicker noise in vortex-based STNOs (in the following called

\*steffen.wittrock@u-psud.fr

†vincent.cros@cnrs-thales.fr

STVOs) both experimentally and theoretically based on the corresponding nonlinear Langevin equations [13] together with a phenomenological approach. Moreover, we present a thorough study of the important parameters governing this type of noise.

In magnetic sensor applications, the flicker noise, which cannot yet be described in its entire universality, is typically described by the empirical Hooge formalism [34,35]. In this work, we also aim at establishing a connection between a magnetic TMR sensor, a fundamental building block of the STNO, and the latter's intrinsic nonlinearity.

We focus our study on vortex-based spin-torque nano-oscillators (STVOs). The fundamental mode in these devices, the gyrotropic vortex motion [36,37], is deterministically well understood and can be described by reducing the complex dynamics to only the dynamics of the vortex core (the so-called Thiele formalism [38]). Moreover, it is energetically well separated from other modes, reducing mode-crossing probabilities. STVOs, compared to other STNOs exploiting different magnetic modes (e.g., a uniform precession or local modes), exhibit large-amplitude oscillations with frequencies from 100 MHz up to  $\sim 1.5$  GHz, a rather narrow linewidth of  $\sim 100$  kHz, and output powers of up to a few microwatts [39]. Since magnetic vortex dynamics has, in many respects, been considered as a model system for the study of magnetic dynamics [22], STVOs are suitable to fundamentally study the noise behavior of STNOs. We believe that the general results of this work can be extrapolated to every kind of STNO, as the nonlinear nature and the basic noise-generating processes are the same. Thus, the main objective is to establish a connection between flicker noise and the STNO's nonlinearity and to study the STNO's flicker noise in general. Such a study has not been performed yet for STNOs, although this is an important issue for the different types of applications aiming to rely on them.

This paper is organized in the following way: We first present the basic mechanisms of the fundamental gyrotropic mode in STVOs. We connect the latter with the general nonlinear auto-oscillator theory, which provides a theoretical basement for the description of STNOs in general. From this model, we deduce the STNO's noise behavior, especially including low offset frequency  $1/f$  flicker noise processes via a phenomenological approach. In Sec. III, we describe the experiment's details and give the basic properties of our samples. In Sec. IV, we present experimental data showing the noise characteristics in STVOs and, subsequently, in Sec. V, focus on the low offset frequency regime. We compare and analyze the experimental data regarding the developed model and, in Sec. V, introduce the formalism of Hooge to discuss the governing parameters of flicker noise in STNOs in general and STVOs in particular.

## II. GENERAL FRAMEWORK OF MAGNETIZATION DYNAMICS AND NOISE IN STNOs AND STVOs

### A. Noise properties of the STVO's gyrotropic mode

In laterally confined geometries such as disks, an excitation of the vortex core from its equilibrium position at the center of the circular nanopillar leads to a radial motion in the subgiga-

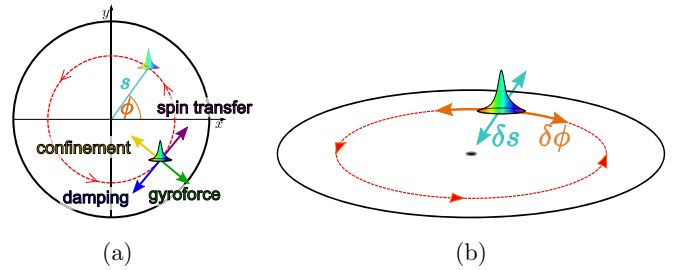


FIG. 1. (a) Schematics of forces acting on the magnetic vortex core: gyroforce (green arrow), confinement force (yellow), spin transfer (purple), and damping force (blue). (b) Noise schematics of vortex motion: amplitude and phase noise,  $\delta s$  and  $\delta \phi$ , respectively.

hertz regime around the equilibrium, i.e., the gyrotropic mode of the vortex core. Assuming the vortex core is a soliton and subsequently applying Thiele's approach [38], this gyrotropic mode is mainly characterized by the vortex core position  $\vec{X}(t)$ , which is represented by the oscillation's orbit radius  $r(t)$ , i.e., its normalized value  $s(t) = r(t)/R$ , and its phase  $\phi(t)$ .

Figure 1(a) schematically summarizes the forces which mainly define the gyrotropic motion within the Thiele formalism [38,40]: the gyroforce, arising from the vortex non-collinear profile, the damping force expressing the magnetic relaxation, the confinement force due to the magnetostatic energy, and the spin transfer force.

As the injected spin transfer torque overcomes the damping, the vortex core auto-oscillates on an isoenergetic trajectory (Fig. 1). Due to the system's nonlinear nature, it is always pushed onto a stable limit cycle as the oscillation amplitude  $a(t) \sim s(t)$  becomes lower than the stable value and is pulled back as it becomes higher.

This limit cycle mechanism also appears in the presence of noise, which perturbs the ideal trajectory and is separated into amplitude and phase noise, as depicted in Fig. 1(b). Noise sources can be manifold and have recently been mainly attributed to thermal origins [12,22,23,41–43], which furthermore lead to a change in spectral shape and an increase in the linewidth of the oscillation [22]. Moreover, the presence of colored  $1/f$  noise has been shown experimentally at offset frequencies close to the carrier [22,23,32,33].

### B. The general nonlinear auto-oscillator theory

We first recall the general nonlinear auto-oscillator theory [13,41,44], which is a universal theoretical approach for nonlinear oscillators in general and STNOs in particular. For STNOs, this model can be derived from the Landau-Lifshitz-Gilbert-Slonczewski equation and describes the deterministic dynamics of the nonlinear oscillator through the complex oscillation amplitude  $c(t) = \sqrt{p(t)}e^{i\phi(t)}$ :

$$\frac{dc}{dt} + i\omega(|c|^2)c + \Gamma_+(|c|^2)c - \Gamma_-(|c|^2)c = f(t). \quad (1)$$

In this model, the gyrotropic motion of the vortex core (as described above) can be identified through the oscillation amplitude  $a(t) = \sqrt{p(t)}$  and phase  $\phi(t)$  of the complex variable  $c(t)$ . Here,  $\omega$  denotes the oscillation's angular frequency,  $\Gamma_+$  is the positive damping rate representing the losses of the

system, and  $\Gamma_-$  is the negative damping rate representing the system's gain.  $f(t)$  is a phenomenological term, which allows a description of the system's interaction with the environment. In the case regarded here, that mainly includes different noise processes, among them thermal and flicker noise, which make Eq. (1) a nonlinear stochastic Langevin equation.

Due to the dependence of the damping parameters on the amplitude ( $\frac{d\Gamma_-(p)}{dp} < 0$  and  $\frac{d\Gamma_+(p)}{dp} > 0$ ), the oscillation is described by a limit cycle with stable oscillation power  $p_0 = |c|^2$ , which is obtained when the positive and negative damping terms are equal:  $\Gamma_-(p) = \Gamma_+(p)$ . Assuming the perturbation  $\delta p$  of the stable oscillation power due to noise gives a characteristic damping rate  $\Gamma_p = \pi f_p = [\frac{d\Gamma_+}{dp}(p_0) - \frac{d\Gamma_-}{dp}(p_0)]p_0$  of small power deviations back to the stable trajectory. The parameter  $\nu = N p_0 / (\pi f_p)$ , with  $N = d\omega(p)/dp$  being the nonlinear frequency shift coefficient, is the normalized dimensionless nonlinear frequency shift and quantifies the coupling between the phase and amplitude due to nonlinearity.

### C. Theoretical description of low offset frequency flicker noise

In the following, we assume a phenomenological ansatz to describe the low offset frequency noise in the framework of the nonlinear auto-oscillator theory. Its parameters can, for STVOs, be identified with the deterministic exploitation of the Thiele equation on the spin-transfer-torque-induced gyrotropic motion [22,40]. More detailed steps of the following derivation can be found in the Supplemental Material [45].

We define  $f_n(t)$ , which is the realization of the stochastic  $1/f$  noise process, to act independently on amplitude and phase  $g_n(t) = \text{Re}[f_n(t)e^{-i\phi(t)}]$  and  $h_n(t) = \text{Im}[f_n(t)e^{-i\phi(t)}]$ . Here, the flicker noise process is assumed to be stationary, and so are  $g_n$  and  $h_n$ . Note that the colored  $1/f$  noise can be modeled from an ensemble of statistically independent Ornstein-Uhlenbeck processes with varying correlation times [46]. Linearization of Eq. (1) with the perturbed oscillator power  $p = p_0 + \delta p$  and the phase fluctuations  $\delta\phi(t)$  gives the coupled differential equations [12,13,24]:

$$\begin{aligned} \frac{d(\delta p)}{dt} + 2\pi f_p \delta p(t) &= 2\sqrt{p_0} g_n(t), \\ \frac{d(\delta\phi)}{dt} &= \frac{1}{\sqrt{p_0}} h_n(t) - N \delta p(t). \end{aligned}$$

Solving in the frequency space yields

$$\delta p(f) = \frac{\sqrt{p_0}}{\pi f_p + i\pi f} g_n(f)$$

and

$$\delta\phi(f) = \frac{1}{2\pi i f \sqrt{p_0}} h_n(f) - \frac{N}{2\pi i f} \delta p(f).$$

Inserting the experimental  $1/f^\gamma$  behavior of the noise spectral density into the autocorrelation's Fourier transform exploiting the Wiener-Khinchine theorem

$$S_{f_n}(f) = \int \langle f_n(t) f_n^*(t-t') \rangle e^{2\pi i f t} dt = \frac{\alpha}{f^\gamma}$$

allows formulating the expression for the power spectral densities (PSDs) of phase and amplitude noise in the low offset frequency regime. Together with the noise PSD resulting from thermal noise processes (as studied in Refs. [12,13,22–24]), we obtain the total noise PSD expression  $S_{\delta\epsilon}$  for the normalized amplitude  $\epsilon = a/a_0 = s/s_0$  and  $S_{\delta\phi}$  for the phase:

$$S_{\delta\epsilon} = \frac{\Delta f_0}{\pi} \frac{1}{f^2 + f_p^2} + \frac{1}{4p_0\pi^2(f_p^2 + f^2)} \frac{\alpha}{f^\gamma}, \quad (2)$$

$$S_{\delta\phi} = \frac{\Delta f_0}{\pi f^2} + \frac{1}{4p_0\pi^2 f^2} \frac{\alpha}{f^\gamma} + \frac{\nu^2 f_p^2}{f^2} S_{\delta\epsilon}. \quad (3)$$

The first terms in both equations, proportional to the oscillation linewidth  $\Delta f_0$ , correspond to thermal origins, whereas all other terms describe the additional PSD due to flicker noise, which is at the center of the present study. Note that the variable  $\alpha$  for the amplitude noise is not necessarily equivalent to  $\alpha$  in the phase noise equation as different mechanisms might contribute.

The flicker noise terms describe the original noise of exponent  $\gamma$ , which leads to a  $1/f^\gamma$  slope for the amplitude and a  $1/f^{\gamma+2}$  slope for the phase noise. Equation (3) clearly shows the nonlinear conversion from amplitude to phase noise. Moreover, we also find an additional, noncoupled pure phase flicker noise term, the second term in Eq. (3), which also exhibits a  $1/f^{\gamma+2}$  characteristic.

## III. EXPERIMENT

The samples are circular-shaped magnetic tunnel junctions of diameter  $2R = 375$  nm, which consist of a pinned layer made of a conventional synthetic antiferromagnetic stack (SAF), a MgO tunnel barrier, and a FeB free layer exhibiting a magnetic vortex configuration. The layers are deposited by ultrahigh-vacuum magnetron sputtering and patterned using  $e$ -beam lithography and Ar ion etching. After annealing at  $360^\circ\text{C}$  for 1 h, the resistance-area product is  $RA \approx 4 \Omega \mu\text{m}^2$ . The TMR ratios lie around 100% at room temperature, with resistance values of  $1/G_0 = (44 - 45) \Omega$  in the vortex state, slightly dependent on the applied current with negative slope. The SAF is composed of PtMn(15)/Co<sub>71</sub>Fe<sub>29</sub>(2.5)/Ru(0.86)/CoFeB(1.6)/Co<sub>70</sub>Fe<sub>30</sub>(0.8), and the total layer stack is SAF/MgO(1)/FeB(4)/MgO(1)/Ta/Ru, with the nanometer layer thickness in parentheses.

The SAF's top magnetic layer exhibits a uniform magnetization in the film plane, which can be slightly tilted by applying an external magnetic field  $H_\perp$  perpendicular to the latter. For all the presented measurements, the field is chosen to be  $\mu_0 H_\perp = 500$  mT. This gives an out-of-plane spin polarization of the injected dc current providing the necessary spin transfer torque component to sustain the gyrotropic vortex motion [47]. Increasing the dc current injected through the layer structure leads to a stronger spin transfer torque counteracting the natural damping of the gyrotropic vortex core motion until, at a certain threshold current value  $I_c$ , the damping is overcome and auto-oscillation of the vortex core around the disk center arises [47].

The TMR effect allows the magnetization dynamics to be converted into an electrical rf signal. In the circuit, the dc

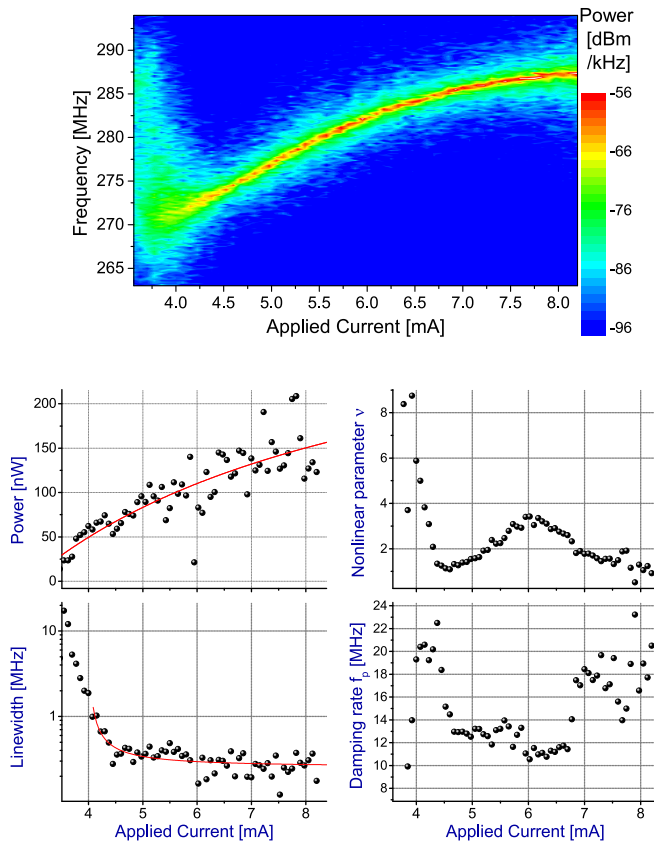


FIG. 2. Characteristic oscillation parameters, such as the oscillation frequency  $f_c$ , output power  $p_0$ , nonlinear parameter  $\nu$ , linewidth  $\Delta f_0$ , and damping rate  $f_p$ , as a function of the applied current  $I_{dc}$  at  $\mu_0 H_{\perp} = 500$  mT.

and rf current parts are separated through a bias tee, and the measured rf signal is evaluated as the direct interpretation of the magnetization dynamics.

The magnitude of the oscillation's output power  $p_0$ , its linewidth  $\Delta f_0$ , and the carrier frequency  $f_c$  (the frequency of the spin-torque-driven magnetization dynamics) are obtained from Lorentzian fits of the emission power spectra, measured by a spectrum analyzer. Noise data are gathered from single-shot oscilloscope voltage time traces and evaluation via the Hilbert transform method [23,48]. To obtain noise data close to the carrier (down to 1 Hz offset), the signal is first down-converted to  $(2 \pm 1)$  MHz via frequency mixing with an external source (see Refs. [32,33]). This allows us to decrease the oscilloscope's sampling rate (from  $\sim 5$  GSample/s down to  $\sim 40$  MSample/s) and to increase the measurement time (from  $\sim 8.2$  ms to  $\sim 2.05$  s) while conserving the signal's noise properties. High-frequency components are filtered by a low-pass filter (bandwidth DC to 22 MHz). More details on the noise measurement and data processing are given in the Supplemental Material [45].

The oscillator's nonlinearity parameters (more explicitly described in Sec. II B) are determined from the oscilloscope's time-space measurements. The damping rate  $f_p$  back to the stable oscillation trajectory is estimated by performing an exponential fit to the signal amplitude's autocorrelation [48]. The nonlinearity parameter  $\nu$ , a measure for the system's

nonlinearity, is obtained by comparing the coupling between amplitude and phase noise as elaborated in Sec. II. In Fig. 2 we present the evaluated basic parameters of the STVO's oscillation at the chosen experimental conditions. In addition, we fit the data with the expected behavior of the magnitudes. The evolution of the power and linewidth with the applied current can be fitted from their theoretical description [13]  $p_0(I) = (I/I_c - 1)/(I/I_c + Q)p_{\max}$  and  $\Delta f_0(I) \sim 1/p_0(I)$ , respectively, with the oscillation threshold current  $I_c \approx 3.7$  mA and  $Q$  and  $p_{\max}$  being the respective fitting parameters. The parameter  $Q$  represents the nonlinearity of the damping (cf. Ref. [13]).

In this work, we restrict the measurements and analysis to the oscillation behavior in the dc current regime corresponding to the gyrotropic mode. In particular, we avoid any perturbing effects of mode crossing (as in Ref. [33]) or more complex dynamical behavior in the regime of very large excitation. Indeed, beyond the stable gyrotropic mode (mode crossing, energy transfer into other subordinate modes), under specific current and field conditions, the occurrence of RTN at characteristic frequencies of up to 10 kHz can be observed. However, this is not investigated further here (and is even particularly avoided), as the detailed analysis of the noise characteristics in the RTN regime goes beyond the scope of this paper.

#### IV. RESULTS: NOISE IN STVOs

A standard visualization of noise properties is the representation of the PSD, which has the advantage of allowing a direct distinction between the underlying noise processes and classifying them by their characteristic inverse power law behavior  $\text{PSD} \sim 1/f^{\beta}$ . In Fig. 3, we show (among other curves explained later) typical measurement data for the phase noise (black curve) and the amplitude noise PSD (gray curve) of the studied STVO sample at an applied current of  $I_{dc} = 4.6$  mA. The noise PSDs are depicted versus the offset  $f_{\text{off}} = |f - f_c|$  from the carrier frequency  $f_c$  (frequency of the vortex gyrotropic motion). The behavior is mainly described by the nonlinear nature of the oscillator. For higher offset frequencies ( $f_{\text{off}} \gtrsim 10^5$  Hz in Fig. 3), the curve's shape is governed by thermal white Gaussian noise processes, thoroughly investigated in Ref. [23] for uniform STNOs (STNOs exploiting the uniform precession of magnetization dynamics) and in Ref. [22] for STVOs (STNOs exploiting the vortex gyrotropic mode). In this region, theoretically represented in the inset of Fig. 3 based on Eqs. (2) and (3) for clarity, the noise signature behaves linearly below the relaxation rate  $f_p$  with exponent  $\beta = 2$  for the phase and  $\beta = 0$  for the amplitude noise. The coupling between the amplitude and phase leads to a conversion of amplitude to phase noise and therefore to an increase in the phase noise by  $10 \log_{10}(1 + \nu^2)$ . For  $f_{\text{off}} \gg f_p$ , perturbations are faster than the nonlinear damping response  $\tau_p = 1/(2\pi f_p)$ , which is usually on the order of a few tens of oscillation periods (depending on the spin-torque strength), so that the nonlinearity becomes less significant. The amplitude noise decreases with  $1/f^2$ , and the phase noise decreases with  $1/f^4$  for  $f_p \ll f_{\text{off}} \ll \nu f_p$  and with  $1/f^2$  for  $f_{\text{off}} \gg \nu f_p$ . At even higher offset frequencies the Johnson-Nyquist noise floor eventually limits the PSDs (not shown in Fig. 3).

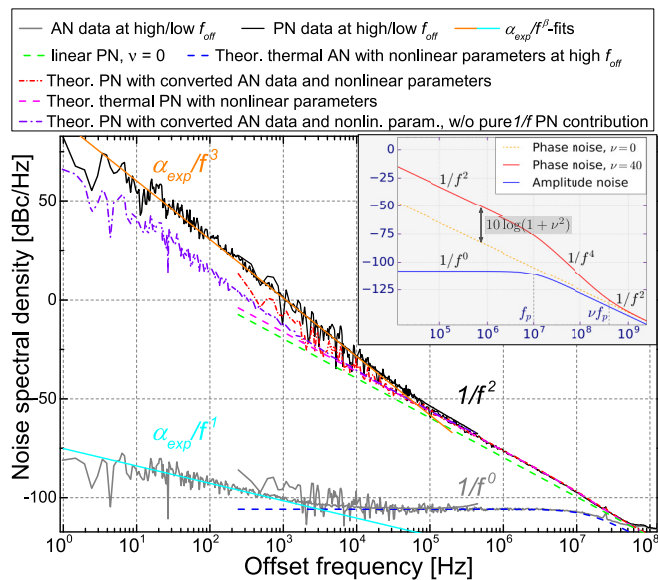


FIG. 3. PSD of phase (PN) and amplitude (AN) noise,  $\mu_0 H_{\perp} = 500$  mT,  $I = 4.6$  mA, as well as theoretical curves based on Eqs. (2) and (3) and described in the text. The inset shows an analytical representation [Eqs. (2) and (3)], but with parameters that are different from the measurement of the higher offset frequency noise due to thermal effects. The phase noise of a linear oscillator ( $\nu = 0$ , dashed line) is shown, along with its increase due to nonlinearity.

For low offset frequencies  $f_{\text{off}} \lesssim 10^4$  Hz, which are the focus of this work, the PSD spectra exhibit a  $1/f^3$  and a  $1/f^1$  behavior for phase and amplitude noise, respectively, where  $1/f$  flicker noise is found to be dominant over thermal noise processes. The fits  $\sim \alpha_{\text{exp}}/f^{\beta}$  to the experimental data in Fig. 3 (orange curve for phase noise and cyan curve for amplitude noise) illustrate the curves' typical slopes and furthermore give the corresponding experimental noise prefactor  $\alpha_{\text{exp}}$ , discussed in Sec. V.

The fundamental origin of flicker noise, described through the phenomenological parameter  $\alpha$  in Eqs. (2) and (3), cannot implicitly be specified as different physical processes are potential origins. This includes intrinsic phenomena such as fluctuations in the magnetic texture [28,29,49], the impact of defects and/or inhomogeneities in the magnetic layers, and the tunnel barrier in particular due to the fabrication process [33]. Even external fluctuations of the driving dc current and the applied magnetic field can play a role.

Comparing the experimental data depicted in Fig. 3 with the theoretical equations (2) and (3), we find for the generating noise process  $\gamma \approx 1$  and a conversion of  $1/f^1$  amplitude into  $1/f^3$  phase noise, reflected both in Fig. 3 (black and gray curves in the low offset frequency regime) and in Eq. (3). Next to the experimental PSDs, Fig. 3 also displays theoretical curves excluding one or more terms in Eqs. (2) and (3), described in the following. The preliminarily evaluated experimental values  $p_0$ ,  $\nu$ ,  $\Delta f_0$ , and  $f_p$ , presented in Fig. 2, are fed into the equations. Considering only the thermal linear part of the phase noise PSD ( $\nu = 0$ , green curve in Fig. 3) again emphasizes the noise growth due to nonlinearity  $\nu > 0$ , as this curve is clearly below the experimental one (black curve

in Fig. 3). For higher offset frequencies (flicker contribution is negligible), theoretical amplitude and phase noise curves (blue dashed and pink dashed curves, respectively) exhibit, as expected, excellent agreement with the corresponding data (black and gray curves, respectively).

For lower offset frequencies, from  $\sim 10^4$  Hz downwards, the flicker noise neglected so far sums to the thermal noise parts and lets the experimental and theoretical curves diverge. The red dot-dashed curve in Fig. 3 describes the theoretical phase noise PSD, including the extra contribution from the conversion of experimental amplitude noise through the coupling term in Eq. (3); thus, it neglects only the pure flicker phase noise term [second term in Eq. (3)]. Importantly, we note that this curve still clearly remains below the experimental data (black curve in Fig. 3) in the range of low offset frequencies but fits well for higher offsets.

## V. RESULTS: ANALYSIS OF THE FLICKER NOISE REGIME

In Fig. 3, we demonstrate that the above-described theoretical curves, based on the thermal noise contribution, correspond well to the experimental data at higher frequencies. At lower offset frequencies ( $f_{\text{off}} \lesssim 10^4$  Hz), they clearly differ. To understand this difference, we further evaluate Eq. (3) using the low offset amplitude noise to additionally consider amplitude-phase coupling and to classify the important parameters in the region  $f_{\text{off}} \lesssim 10^4$  Hz. Hence, the violet curve in Fig. 3 represents the phase noise including only the thermal and amplitude-converted contributions (similar to the red dot-dashed curve in the high offset frequency regime). The difference between the experimental phase noise PSD (black curve in Fig. 3) and the calculated curve (violet) therefore clearly pinpoints the pure phase flicker noise in Fig. 3, which is found to be dominant against the other contributions. To further classify the important noise parameters, we concentrate on the pure phase flicker noise in the following.

In Fig. 4, we compare the experimental prefactors  $\alpha_{\text{exp}}$  of the  $\alpha_{\text{exp}}/f^{\beta}$  fits to the experimental low-frequency noise, as depicted in Fig. 3, and plot them as a function of the injected dc current. The green points in Fig. 4 represent the difference between the experimental data curve (black curve in Fig. 3) and the data curve including thermal noise and nonlinear amplitude noise conversion (violet curve in Fig. 3), notably the pure phase flicker noise. The difference between the two curves (red and green points in Fig. 4) directly reflects the contribution from the part of the noise which is converted from amplitude to phase. Indeed, this difference is small and therefore emphasizes that the pure flicker phase noise is dominant for the flicker noise regime. This conclusion is one of the important results of this work.

### Governing parameters and relation to the Hooge formalism

Another important result is that the flicker noise for both the amplitude noise (blue points in the bottom panel of Fig. 4) and the phase noise (red and green points in Fig. 4) decreases as the injected dc current is increased. For comparison, this behavior is different from what is found in conventional TMR sensors [28,35,50], whose layer structure is very similar to that of STNOs. For these devices, the low-frequency noise

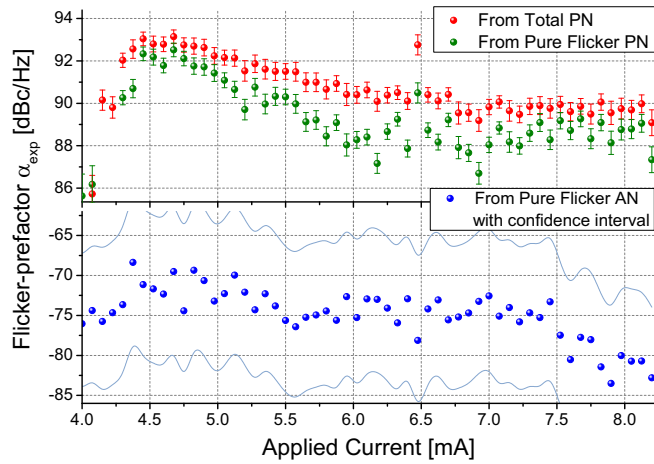


FIG. 4. Evolution with applied current of the prefactors  $\alpha_{\text{exp}}$  from the  $\alpha_{\text{exp}}/f^\beta$  fits of (i) the experimental phase noise (PN) data (red points), (ii) the pure flicker PN (difference between black and violet curves in Fig. 3), represented by green points, and (iii) the amplitude noise (AN) data (blue points).

behavior is usually evaluated only by a description based on the phenomenological Hooge formula [34,35]:

$$S_P = \frac{\alpha_H P_{dc}}{A f^\beta}, \quad (4)$$

with  $P_{dc}$  being the circuit's dc power,  $A$  being the magnetically active surface, which is usually constant in TMR sensors, and  $\alpha_H$  being the Hooge parameter. Interestingly, the coefficient  $\alpha_H$  is often considered a kind of quality factor, e.g., in magnetic sensor technologies. It includes the intrinsic origins of the flicker noise due to the manifold potential mechanisms already mentioned before.

Note that the phenomenological Hooge formula was originally well adapted to semiconductor devices [51–53]. There, it describes the  $1/f$  noise proportional to the power supplied to the system averaged over the number of carriers. By applying the Hooge model to magnetic sensors, the averaging is indeed realized on the effective magnetic volume that is converted into the active magnetic surface  $A$  after proper renormalization in Eq. (4). In STVOs, the nonlinear evolution of the active surface  $A$  or, more generally, the active magnetic volume has to be especially taken into account, as, usually, not all the device area is active; only the surface enclosed by the vortex core trajectory contributes to the rf signal (red circle in Fig. 1). A particularity of STVOs (and STNOs in general) is that, resulting from the nonlinearities of the different forces acting on the vortex core,  $A$  can be controlled by the amplitude of the spin transfer torque.

The active surface  $A = \pi(Rs_0)^2$  can be experimentally determined by measuring the conductivities in the vortex and antiparallel state  $G_0(I_{dc})$  and  $G_{ap}(I_{dc})$ , the TMR value  $\text{TMR}(I_{dc})$ , the corresponding applied field values  $h_i$  normalized to the magnetization of layer  $i$ , and the effective oscillation voltage  $V_{rf}$  [22]. In the vortex oscillator model system,

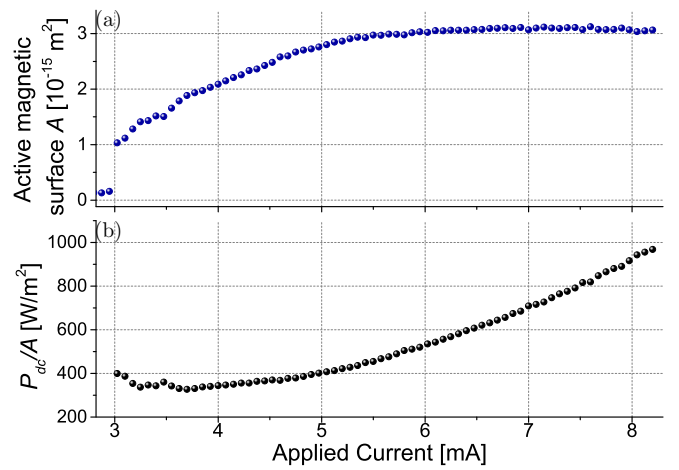


FIG. 5. (a) Experimental active magnetic surface  $A$  and (b) Hooge proportionality  $P_{dc}/A$  vs applied dc current  $I_{dc}$ .

the oscillation radius can be calculated through

$$s_0 = \frac{2G_0(1 + G_0Z_{50\Omega})}{I_{dc}\text{TMR}(I_{dc})G_{ap}Z_{50\Omega}\lambda} \times \frac{1}{\sqrt{(1 - h_{\text{free}}^2)(1 - h_{\text{SAF}}^2)}} V_{rf0},$$

with  $Z_{50\Omega}$  being the load and  $\lambda \approx 2/3$  being a magnetoresistive factor (the proportionality factor for the planar magnetization value relative to the saturation magnetization). Note that the average resistance  $1/G_0 = R_0(I_{dc})$  usually decreases for larger currents.

The evaluated active surface of the studied STVO as a function of the dc current is shown in Fig. 5, along with the Hooge proportionality  $P_{dc}/A$ , which mainly determines the noise prefactor in Eq. (4).

We find that the Hooge proportionality  $P_{dc}/A$  is first constant and then increases as a function of  $I_{dc}$ . For lower currents, the evolution of  $A$  is, in fact, compensating the increase. But then in the regime of constant  $A$ , the quadratic behavior of  $P_{dc}/A$  is similar to what is usually found in magnetic TMR/GMR sensors. Following the Hooge model, a consequence is that the noise level for higher currents will also increase. As shown in Fig. 4, this is contrary to what we find experimentally. Thus, we conclude that  $P_{dc}/A$  alone does not properly describe the flicker noise behavior of a STVO like it mainly does in the case of magnetic sensors.

Indeed, the nonlinear nature of the oscillator, expressed by Eqs. (2) and (3), has to be taken into account. It obviously dominates over the Hooge behavior, which is, in fact, valid for the static case with no sustained dynamics. In Eqs. (2) and (3) we assume the generating noise (which is not deterministically understood so far) follows Hooge's description in Eq. (4) and include it in the parameter  $\alpha \sim \alpha_H P_{dc}/A$ . Note that the prefactor  $\alpha_H$  for the phase does not necessarily need to be equivalent to that of the amplitude noise.

In Fig. 6, we calculate the evolution of the flicker noise prefactor vs  $I_{dc}$  based on the parameters of Eqs. (2) and (3), taking into account the previously discussed effects. At this stage, we neglect  $\alpha_H$ , which will be discussed later,

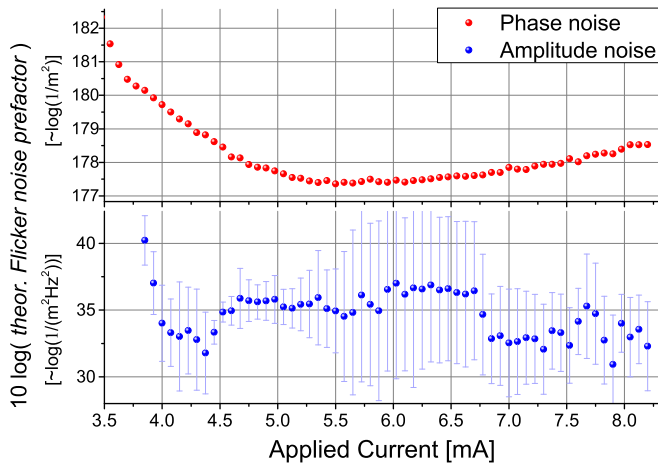


FIG. 6. Calculated pure flicker noise prefactors evaluated through Eqs. (2) and (3) with measured experimental magnitudes without  $\alpha_H$ .

and therefore plot  $P_{dc}/(4p_0\pi^2 f_p^2 A)$  for the amplitude and  $P_{dc}/(4p_0\pi^2 A)$  for the pure phase flicker noise prefactor. The calculated noise prefactors of the pure amplitude and phase flicker noise terms (Fig. 6) qualitatively reproduce the trends of the direct measurement, represented in Fig. 4. In particular, we see that the phase noise curve first decreases, then remains constant over a certain current range until it starts increasing again from  $\sim 6.5$  mA on. This behavior is associated with the decreasing nonlinearity at higher currents [22] and a resulting nearly constant oscillation radius  $s_0$  and output power  $p_0$  in this regime (compare Figs. 5 and 2). Therefore, the Hooge ratio  $P_{dc}/A$  also becomes more influential and starts to dominate the noise behavior in a way similar to what is usually found in TMR sensors.

The amplitude noise prefactor (Fig. 6, blue curve) is slightly decreasing in the range of the experimentally studied injected currents, but it has to be remarked that the error bars are large. In general, the flicker contribution of  $S_{\delta\epsilon}$  mainly depends on the damping rate  $f_p$  back to the limit cycle.

The Hooge parameter  $\alpha_H$  (not yet considered for the data shown in Fig. 6) can be estimated from our results as a proportionality factor between the calculated noise prefactors (shown in Fig. 6) and the measured values (shown in Fig. 4). We estimate  $\alpha_{H,\delta\phi} \approx 10^3 \Omega \mu\text{m}^2 \Leftrightarrow G_0\alpha_{H,\delta\phi} \approx 10^1 \mu\text{m}^2$  for the phase and  $\alpha_{H,\delta\epsilon} \approx 10^1 \Omega \mu\text{m}^2 \Leftrightarrow G_0\alpha_{H,\delta\epsilon} \approx 10^{-1} \mu\text{m}^2$  for the amplitude noise. For comparison, in TMR-based sensors the obtained values are typically between  $G_0\alpha_H \approx 10^{-6} \mu\text{m}^2$  [28,54] and  $10^{-11} \mu\text{m}^2$  [29,55–57], measured for voltage fluctuations upon the tunnel junction. In Ref. [29],  $G_0\alpha_H \approx 10^{-11} \mu\text{m}^2$  is calculated from data on TMR sensor devices with a layer structure similar to ours and a resistance-area product  $RA$  well below  $100 \text{ k}\Omega \mu\text{m}^2$ , where  $\alpha_H$  usually becomes stable in terms of  $RA$  [35]. In contrast to the present work, data in Ref. [29] were obtained at low temperature ( $T = 5$  K). Thermal noise processes can also be the generator of  $1/f$  noise processes (Barkhausen noise), as shown in Ref. [57], where a decrease in  $\alpha_H$  by about 2 orders of magnitude at low compared to room temperature was measured. Moreover, we apply up to  $\sim 400$  mV compared to a maximum bias

voltage of  $\sim 50$  mV in Ref. [29]. Usually,  $\alpha_H$  decreases with higher applied voltages by up to one order of magnitude [54–56] due to new conductance channels arising in this range of biases (and the likewise decreasing TMR ratio) [54,56]. In our devices, this behavior leads to a suppression of the phase noise increase for higher currents, as presented in Fig. 6. Finally, the parameter  $\alpha_H$  in general depends on the magnetic configuration of the magnetic tunnel junction [in sensors mainly parallel (P) and antiparallel (AP)] because of the different nature of tunneling channels. The higher noise level in the AP state can [57] be mostly explained by a higher contribution to noise from tunneling electrons from the localized bands. Those are more sensitive to charge traps (e.g., magnetic impurities) in the insulator. In the AP state, mainly localized bands contribute to the tunneling compared to mainly delocalized  $s$  electrons in the P state. Therefore, the difference in the Hooge parameter  $\alpha_{H,AP} > \alpha_{H,P}$  is usually at least a factor of 2 [35] but more often even 1 or 2 orders of magnitude [55,56,58].

As an important result, we state that the system’s nonlinear nature strongly governs not only the thermal but also the flicker noise behavior. The influence on the statically observed noise proportionality  $P_{dc}/A$ , which is modeled by the Hooge formalism, is found to be of minor significance, at least until the larger current regime where the nonlinearity decreases and oscillation radius  $s_0$  and oscillation output power  $p_0$  do not significantly increase anymore. In this regime, the phase noise follows a Hooge-like increase, as we find in the evolution of the calculated parameters. Note, however, that this trend is found to be much less pronounced in the parameters extracted from the measurements (see Fig. 4) due to the evolution of  $\alpha_H$  expected in this range of very large applied biases. In fact, the phenomenological parameter  $\alpha_H$  describes the noise level and may have contributions from both magnetic and electronic mechanisms (as well as the microstructural quality of the thin films [33]) that might differ for amplitude and phase. A comparison with known values in similar TMR devices usually operating at very low voltage bias is not straightforward, because as we show here, all noise mechanisms might act in fundamentally different ways. As we demonstrate, the evolution of the output power  $p_0$  and the (correlated) active magnetic surface  $A$  are essential for the phase noise. For the amplitude noise, the essential governing parameter is the damping rate  $f_p$  back to the limit cycle.

## VI. CONCLUSION

We presented here a phenomenological theory based on the nonlinear auto-oscillator model in order to describe the noise properties of spin-torque nano-oscillators in the low offset frequency range. We investigated how the  $1/f$  flicker noise, which is the dominant noise source in the low offset frequency regime, is connected to the oscillator’s nonlinear dynamics.

In addition to the theoretical description, we also conducted a detailed experimental investigation performed on vortex-based spin-torque oscillators and discussed the results based on the theoretical predictions. We measured a  $1/f^1$  flicker amplitude noise and its conversion into  $1/f^3$  phase noise. Indeed, the phase noise additionally exhibits a

pure phase flicker noise contribution, which is found to be dominant. As a consequence, we hence demonstrated that the amplitude-phase-noise coupling is less important in the low offset frequency regime compared to higher-frequency offsets.

In summary, we found that the flicker noise in spin-torque oscillators, particularly in STVOs but extendable to other STNOs, is determined by the system's nonlinear parameters in the highly frequency tunable operation range. We also showed that this conclusion becomes less valid in the regime of very large driving force on the vortex core (i.e., large applied current). Moreover, we combined the dynamical equations with the well-established Hooge formalism for TMR sensors

and emphasized the importance of different parameters on the low offset frequency noise.

We believe that our work contributes to the fundamental understanding of the  $1/f$  flicker noise in spin-torque nano-oscillators. As this noise type especially limits the spin-torque oscillator's long-term stability, we furthermore believe that this work provides a basis to improve the noise characteristics of various applications aiming to rely on STNO devices.

#### ACKNOWLEDGMENTS

S.W. acknowledges financial support from Labex FIRST-TF. The work is supported by the French ANR project "SPIN-NET" ANR-18-CE24-0012.

- 
- [1] M. N. Baibich, J. M. Broto, A. Fert, F. Nguyen Van Dau, F. Petroff, P. Etienne, G. Creuzet, A. Friederich, and J. Chazelas, *Phys. Rev. Lett.* **61**, 2472 (1988).
- [2] G. Binasch, P. Grünberg, F. Saurenbach, and W. Zinn, *Phys. Rev. B* **39**, 4828 (1989).
- [3] L. Berger, *Phys. Rev. B* **54**, 9353 (1996).
- [4] J. Slonczewski, *J. Magn. Magn. Mater.* **159**, L1 (1996).
- [5] S. I. Kiselev, J. C. Sankey, I. N. Krivorotov, N. C. Emley, R. J. Schoelkopf, R. A. Buhrman, and D. C. Ralph, *Nature (London)* **425**, 380 (2003).
- [6] N. Locatelli, V. Cros, and J. Grollier, *Nat. Mater.* **13**, 11 (2013).
- [7] B. Fang, M. Carpentieri, S. Louis, V. Tiberkevich, A. Slavin, I. N. Krivorotov, R. Tomasello, A. Giordano, H. Jiang, J. Cai, Y. Fan, Z. Zhang, B. Zhang, J. A. Katine, K. L. Wang, P. K. Amiri, G. Finocchio, and Z. Zeng, *Phys. Rev. Appl.* **11**, 014022 (2019).
- [8] A. S. Jenkins, R. Lebrun, E. Grimaldi, S. Tsunegi, P. Bortolotti, H. Kubota, K. Yakushiji, A. Fukushima, G. de Loubens, O. Klein, S. Yuasa, and V. Cros, *Nat. Nanotechnol.* **11**, 360 (2016).
- [9] S. Louis, V. Tyberkevych, J. Li, I. Lisenkov, R. Khymyn, E. Bankowski, T. Meitzler, I. Krivorotov, and A. Slavin, *IEEE Trans. Magn.* **53**, 1 (2017).
- [10] J. Torrejon, M. Riou, F. A. Araujo, S. Tsunegi, G. Khalsa, D. Querlioz, P. Bortolotti, V. Cros, K. Yakushiji, A. Fukushima, H. Kubota, S. Yuasa, M. D. Stiles, and J. Grollier, *Nature (London)* **547**, 428 (2017).
- [11] M. Romera, P. Talatchian, S. Tsunegi, F. Abreu Araujo, V. Cros, P. Bortolotti, J. Trastoy, K. Yakushiji, A. Fukushima, H. Kubota, S. Yuasa, M. Ernoult, D. Vodenicarevic, T. Hirtzlin, N. Locatelli, D. Querlioz, and J. Grollier, *Nature (London)* **563**, 230 (2018).
- [12] J.-V. Kim, V. Tiberkevich, and A. N. Slavin, *Phys. Rev. Lett.* **100**, 017207 (2008).
- [13] A. Slavin and V. Tiberkevich, *IEEE Trans. Magn.* **45**, 1875 (2009).
- [14] R. Lebrun, A. Jenkins, A. Dussaux, N. Locatelli, S. Tsunegi, E. Grimaldi, H. Kubota, P. Bortolotti, K. Yakushiji, J. Grollier, A. Fukushima, S. Yuasa, and V. Cros, *Phys. Rev. Lett.* **115**, 017201 (2015).
- [15] A. Hamadeh, N. Locatelli, V. V. Naletov, R. Lebrun, G. de Loubens, J. Grollier, O. Klein, and V. Cros, *Appl. Phys. Lett.* **104**, 022408 (2014).
- [16] S. Kaka, M. R. Pufall, W. H. Rippard, T. J. Silva, S. E. Russek, and J. A. Katine, *Nature (London)* **437**, 389 (2005).
- [17] N. Locatelli, A. Hamadeh, F. A. Araujo, A. D. Belanovsky, P. N. Skirdkov, R. Lebrun, V. V. Naletov, K. A. Zvezdin, M. Muñoz, J. Grollier, O. Klein, V. Cros, and G. de Loubens, *Sci. Rep.* **5**, 17039 (2015).
- [18] R. Lebrun, S. Tsunegi, P. Bortolotti, H. Kubota, A. S. Jenkins, M. Romera, K. Yakushiji, A. Fukushima, J. Grollier, S. Yuasa, and V. Cros, *Nat. Commun.* **8**, 15825 (2017).
- [19] A. A. Tulapurkar, Y. Suzuki, A. Fukushima, H. Kubota, H. Maehara, K. Tsunekawa, D. D. Djayaprawira, N. Watanabe, and S. Yuasa, *Nature (London)* **438**, 339 (2005).
- [20] S. Miwa, S. Ishibashi, H. Tomita, T. Nozaki, E. Tamura, K. Ando, N. Mizuochi, T. Saruya, H. Kubota, K. Yakushiji, T. Taniguchi, H. Imamura, A. Fukushima, S. Yuasa, and Y. Suzuki, *Nat. Mater.* **13**, 50 (2013).
- [21] H. Naganuma, G. Kim, Y. Kawada, N. Inami, K. Hatakeyama, S. Iihama, K. M. N. Islam, M. Oogane, S. Mizukami, and Y. Ando, *Nano Lett.* **15**, 623 (2015).
- [22] E. Grimaldi, A. Dussaux, P. Bortolotti, J. Grollier, G. Pillet, A. Fukushima, H. Kubota, K. Yakushiji, S. Yuasa, and V. Cros, *Phys. Rev. B* **89**, 104404 (2014).
- [23] M. Quinsat, D. Gusakova, J. F. Sierra, J. P. Michel, D. Houssameddine, B. Delaet, M.-C. Cyrille, U. Ebels, B. Dieny, L. D. Buda-Prejbeanu, J. A. Katine, D. Mauri, A. Zeltser, M. Prigent, J.-C. Nallatamby, and R. Sommet, *Appl. Phys. Lett.* **97**, 182507 (2010).
- [24] T. J. Silva and M. W. Keller, *IEEE Trans. Magn.* **46**, 3555 (2010).
- [25] E. Rubiola, *Phase Noise and Frequency Stability in Oscillators* (Cambridge University Press, Cambridge, 2008).
- [26] J. B. Johnson, *Phys. Rev.* **26**, 71 (1925).
- [27] J. Bernamont, *Proc. Phys. Soc.* **49**, 138 (1937).
- [28] E. R. Nowak, M. B. Weissman, and S. S. P. Parkin, *Appl. Phys. Lett.* **74**, 600 (1999).
- [29] T. Arakawa, T. Tanaka, K. Chida, S. Matsuo, Y. Nishihara, D. Chiba, K. Kobayashi, T. Ono, A. Fukushima, and S. Yuasa, *Phys. Rev. B* **86**, 224423 (2012).
- [30] J. M. Almeida, R. Ferreira, P. P. Freitas, J. Langer, B. Ocker, and W. Maass, *J. Appl. Phys.* **99**, 08B314 (2006).
- [31] Z. Feng, J. Hu, L. Sun, B. You, D. Wu, J. Du, W. Zhang, A. Hu, Y. Yang, D. M. Tang, B. S. Zhang, and H. F. Ding, *Phys. Rev. B* **85**, 214423 (2012).

- [32] M. W. Keller, M. R. Pufall, W. H. Rippard, and T. J. Silva, *Phys. Rev. B* **82**, 054416 (2010).
- [33] A. Eklund, S. Bonetti, S. R. Sani, S. M. Mohseni, J. Persson, S. Chung, S. A. H. Banuazizi, E. Iacocca, M. Östling, J. Åkerman, and B. G. Malm, *Appl. Phys. Lett.* **104**, 092405 (2014).
- [34] F. N. Hooge and A. M. H. Hoppenbrouwers, *Physica* **45**, 386 (1969).
- [35] C. Fermon and M. Pannetier-Lecoeur, in *Giant Magnetoresistance (GMR) Sensors: From Basis to State-of-the-Art Applications*, Smart Sensors, Measurement and Instrumentation Vol. 6, edited by C. Reig, S. Cardoso, and S. Mukhopadhyay (Springer, Berlin, 2013), pp. 47–70.
- [36] R. P. Cowburn, D. K. Koltsov, A. O. Adeyeye, M. E. Welland, and D. M. Tricker, *Phys. Rev. Lett.* **83**, 1042 (1999).
- [37] T. Shinjo, T. Okuno, R. Hassdorf, K. Shigeto, and T. Ono, *Science* **289**, 930 (2000).
- [38] A. A. Thiele, *Phys. Rev. Lett.* **30**, 230 (1973).
- [39] S. Tsunegi, H. Kubota, K. Yakushiji, M. Konoto, S. Tamaru, A. Fukushima, H. Arai, H. Imamura, E. Grimaldi, R. Lebrun, J. Grollier, V. Cros, and S. Yuasa, *Appl. Phys. Express* **7**, 063009 (2014).
- [40] A. Dussaux, A. V. Khvalkovskiy, P. Bortolotti, J. Grollier, V. Cros, and A. Fert, *Phys. Rev. B* **86**, 014402 (2012).
- [41] V. Tiberkevich, A. Slavin, and J.-V. Kim, *Appl. Phys. Lett.* **91**, 192506 (2007).
- [42] K. Kudo, T. Nagasawa, R. Sato, and K. Mizushima, *J. Appl. Phys.* **105**, 07D105 (2009).
- [43] B. Georges, J. Grollier, V. Cros, A. Fert, A. Fukushima, H. Kubota, K. Yakushiji, S. Yuasa, and K. Ando, *Phys. Rev. B* **80**, 060404(R) (2009).
- [44] A. Slavin and V. Tiberkevich, *IEEE Trans. Magn.* **44**, 1916 (2008).
- [45] See Supplemental Material at <http://link.aps.org/supplemental/10.1103/PhysRevB.99.235135> for details on (a) the noise measurement and (b) the derivation of the noise equations.
- [46] F. X. Kaertner, *Int. J. Circuit Theory Appl.* **18**, 485 (1990).
- [47] A. Dussaux, B. Georges, J. Grollier, V. Cros, A. V. Khvalkovskiy, A. Fukushima, M. Konoto, H. Kubota, K. Yakushiji, S. Yuasa, K. A. Zvezdin, K. Ando, and A. Fert, *Nat. Commun.* **1**, 8 (2010).
- [48] L. Bianchini, S. Cornelissen, J.-V. Kim, T. Devolder, W. van Roy, L. Lagae, and C. Chappert, *Appl. Phys. Lett.* **97**, 032502 (2010).
- [49] Z. Diao, E. R. Nowak, K. M. Haughey, and J. M. D. Coey, *Phys. Rev. B* **84**, 094412 (2011).
- [50] D. Herranz, F. Bonell, A. Gomez-Ibarlucea, S. Andrieu, F. Montaigne, R. Villar, C. Tiusan, and F. G. Aliev, *Appl. Phys. Lett.* **96**, 202501 (2010).
- [51] A. van der Ziel, *Proc. IEEE* **76**, 233 (1988).
- [52] V. K. Sangwan, H. N. Arnold, D. Jariwala, T. J. Marks, L. J. Lauhon, and M. C. Hersam, *Nano Lett.* **13**, 4351 (2013).
- [53] A. Balandin, K. Wang, A. Svizhenko, and S. Bandyopadhyay, *IEEE Trans. Electron Devices* **46**, 1240 (1999).
- [54] A. Gokce, E. R. Nowak, S. H. Yang, and S. S. P. Parkin, *J. Appl. Phys.* **99**, 08A906 (2006).
- [55] J. M. Almeida, P. Wisniowski, and P. P. Freitas, *IEEE Trans. Magn.* **44**, 2569 (2008).
- [56] F. G. Aliev, R. Guerrero, D. Herranz, R. Villar, F. Greullet, C. Tiusan, and M. Hehn, *Appl. Phys. Lett.* **91**, 232504 (2007).
- [57] J. Scola, H. Polovy, C. Fermon, M. Pannetier-Lecœur, G. Feng, K. Fahy, and J. M. D. Coey, *Appl. Phys. Lett.* **90**, 252501 (2007).
- [58] D. Herranz, A. Gomez-Ibarlucea, M. Schäfers, A. Lara, G. Reiss, and F. G. Aliev, *Appl. Phys. Lett.* **99**, 062511 (2011).